Journal of Nuclear Materials 405 (2010) 177–180

Contents lists available at ScienceDirect

Journal of Nuclear Materials

journal homepage: www.elsevier.com/locate/jnucmat

Irradiation-induced changes of the atomic distributions around the interfaces of carbides in a nuclear reactor pressure vessel steel

T. Toyama [a,*], N. Tsuchiya [a], Y. Nagai [a], A. Almazouzi [b,1], M. Hatakeyama [a], M. Hasegawa [c], T. Ohkubo [d], E. van Walle [b], R. Gerard [e]

[a] International Research Center for Nuclear Materials Science, Institute for Materials Research, Tohoku University, Oarai, Ibaraki 311-1313, Japan
[b] SCK-CEN, Nuclear Materials Science Institute, Boeretang 200, 2400 Mol, Belgium
[c] Cyclotron and Radioisotope Center, Tohoku University, Sendai, Miyagi 980-8578, Japan
[d] National Institute for Materials Science, Sengen, Tsukuba 305-0047, Japan
[e] Tractebel Engineering, Avenue Ariane, 1200 Brussels, Belgium

ARTICLE INFO

Article history:
Received 9 March 2010
Accepted 13 August 2010

ABSTRACT

Irradiation-induced changes of the atomic distributions of solute and impurity elements around carbides in a reactor pressure vessel steel of a Belgium nuclear power reactor were investigated by laser-assisted local electrode-type three-dimensional atom probe, before and after in-service irradiation of 12 years. Before irradiation, nano-scale Fe–Mn–Cr–Mo carbides were found to be intragranular. The atomic distributions of Mn, Cr and Mo inside the carbide indicate that their concentrations around the inner carbide–matrix interface were enhanced, while a clear segregation of P at the interface was observed. After irradiation, the Mn concentration in the carbide increased substantially. In addition, the enhancement of Mn, Cr and Mo concentrations around the interface and the segregation of P were markedly intensified.

1. Introduction

The irradiation-induced embrittlement of the nuclear reactor pressure vessel (RPV) steels, low alloy ferritic steels in Western-type light-water reactors, is one of the main issues limiting the end of life of the reactors. Therefore extensive studies have been made worldwide to clarify the mechanisms of the embrittlement. So far, it is widely known that the embrittlement can be classified into two categories; hardening and non-hardening embrittlement [1–3]. The hardening one is due to irradiation-induced solute/impurity precipitates and so-called matrix defects such as interstitial loops and/or nanovoids [1–4]. The non-hardening one is due to irradiation-induced segregation of impurity elements such as P at grain boundaries [1–3,5], carbide–matrix interfaces [6–8] and so on. However, the nanostructural origins of the non-hardening embrittlement have not been fully understood yet.

In the case of cleavage fracture in the brittle metallic materials, micro-crack nucleation initiates at a stress concentrated site. For ferritic steels, carbides or carbide–matrix interfaces are the typical initiation sites of the cleavage micro-crack nucleation [9,10]. A recent fracture toughness prediction model suggests that the strength of carbide–matrix interface is reduced when the concentrations of impurity element such as P around the carbides increase [6,11,12]. Thus we should take notice of irradiation-induced changes of the atomic distributions of solute and impurity elements around carbide–matrix interfaces.

On the carbides in RPV steels, conventional scanning and transmission electron microscopes have previously characterized their size distributions [13] and structures [14]. Furthermore, atom probe (AP) enables us to analyze nanostructures of carbides by mapping out atomic distributions with atomic scale resolution. Several AP works have investigated cementite carbides (M_3C) and Mo carbides (MoC and Mo_2C) in RPV steels [15–18]: the shapes and chemical compositions of the carbides have been reported. However, to the best of our knowledge, detailed analyses on the atomic distributions around carbide–matrix interfaces have rarely been reported in the open literature. Here we employ a laser-assisted local electrode-type three-dimensional AP (3D-AP) to observe the nanostructure of the carbides. A laser-assisted local electrode-type 3D-AP has two marked advantages over a conventional 3D-AP: much larger field of view with high data collection rate [19] and lower specimen fracture probability with laser pulse evaporation even for brittle specimens [20,21]. In this paper, we show the irradiation-induced changes of the atomic distributions around the interfaces of nano-carbides in a surveillance test specimen of a RPV steel of a Belgium nuclear power reactor.

* Corresponding author. Tel.: +81 29 267 3181; fax: +81 29 267 4947.
E-mail address: ttoyama@imr.tohoku.ac.jp (T. Toyama).
[1] Present address: EDF R&D, Les Renardières, MoretsurLoing, France.

0022-3115/$ - see front matter © 2010 Elsevier B.V. All rights reserved.
doi:10.1016/j.jnucmat.2010.08.011

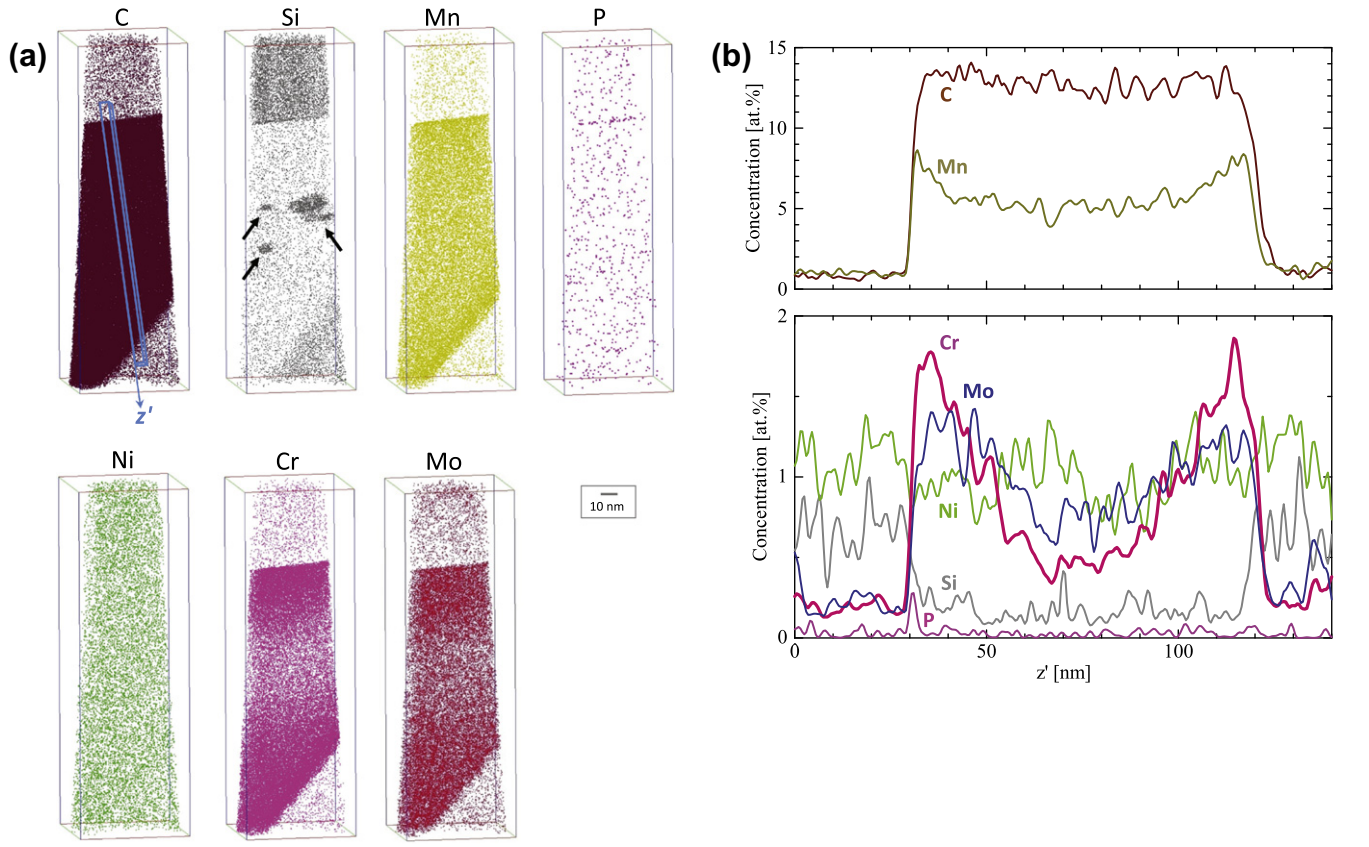

Fig. 1. (a) Elemental maps of solute atoms around the carbide in the unirradiated specimen, and (b) concentration profiles of each element as a function of position across one of the carbide–matrix interfaces in the selected region of a rectangular parallelepiped of 5 × 5 nm cross section in Fig. 1a.

Table 1
Chemical composition of the surveillance test specimen (balance: Fe).

	C	Si	Mn	P	Cu	Ni	Cr	Mo
at.%	0.9	0.56	1.45	0.014	0.04	0.71	0.12	0.31
wt.%	0.2	0.28	1.43	0.008	0.05	0.75	0.11	0.53

2. Experimental

The studied surveillance test specimen of low alloy ferritic alloy A508 was obtained from the surveillance program of Doel-4 reactor in Belgium operating since 1985. The chemical composition of the specimen is listed in Table 1 in atomic and weight percent. This is the typical second generation RPV steels characterized by lower impurity concentrations of such as P, S and Cu. The specimen was in-service irradiated to a neutron dose of 3.3×10^{19} n cm^{-2}, for about 12 years, with a flux of 1.3×10^{11} n cm^{-2} s^{-1} ($E > 1$ MeV) at ~300 °C. The same material of unirradiated (the archive specimen) was also investigated for comparison with the irradiated one.

For 3D-AP observation, the rod samples were prepared from the test specimens using an electrodischarge cutter in order to minimize possible cutting-induced surface damage. Then the rods were electro-polished to needles with a solution of 2-butoxyethanol with 2% perchloric acid. Finally focused ion beam (FIB) with scanning electron microscope was applied to set the carbide near the top of the needle tip. 3D-AP observation was carried out with LEAP-3000XHR by IMAGO Scientific Instruments, under conditions of a laser power of 0.5 nJ, a laser pulse repetition rate of 200 kHz, a DC voltage usually in a range from 5 to 10 kV and a specimen temperature of 30 K.

3. Results and discussions

Elemental maps of various kinds of solute atoms around the carbide in the archive specimen are shown in Fig. 1a. The observed carbide was in a nano-scale dimension and was enriched with Mn, Cr and Mo; Nano-scale Fe–Mn–Cr–Mo carbide. Ni, a non-carbide-forming element [22,23], was hardly enriched. P was segregated at the carbide–matrix interface. Si was depleted in the carbide, which is similar to the case of cementites [23–25], but small silicides were observed as indicated by the arrows. Average concentrations of the each element in the carbide other than the silicides are as follows; C: ~13%, Si: ~0.2%, Mn: ~6%, Ni: ~1%, Cr: ~1%, Mo: ~1% and balanced Fe (78%). All the concentrations are given in atomic percent. Subtotal concentration of the metal elements (Mn + Cr + Mo + Fe) is about 86%, which is close to that of M_6C type carbide, one of the typical carbides in low alloy ferritic steels.

Fig. 1b shows concentration profiles of each element as a function of distance in the selected region as shown in the C map in Fig. 1a, a blue rectangular parallelepiped of 5 × 5 nm cross section. The C concentration was ~13% throughout the carbide. On the other hand, the Mn, Cr and Mo concentrations were enhanced around the inner carbide–matrix interface. The Mn concentration was ~5% around the center of the carbide (z' = 60–90 nm) while ~8% around the interface ($z' \sim 30$ nm and $z' \sim 20$ nm). The full width at half maximum (FWHM) of the enhancement peaks of Mn at the interface ($z' \sim 30$ nm) was estimated to be ~7 nm. In the similar way, FWHM of the enhancement peaks of Cr and Mo at the interface were roughly estimated as ~15 nm and ~20 nm, respectively.

Elemental maps of the solute atoms around the carbide in the irradiated surveillance test specimen are shown in Fig. 2a. The carbide was enriched with Mn, Cr and Mo. The depletion of Si and the segregation of P at the carbide–matrix interface were also seen after irradiation. A small silicide was observed as indicated by the arrow. These characteristics associated with the carbide were

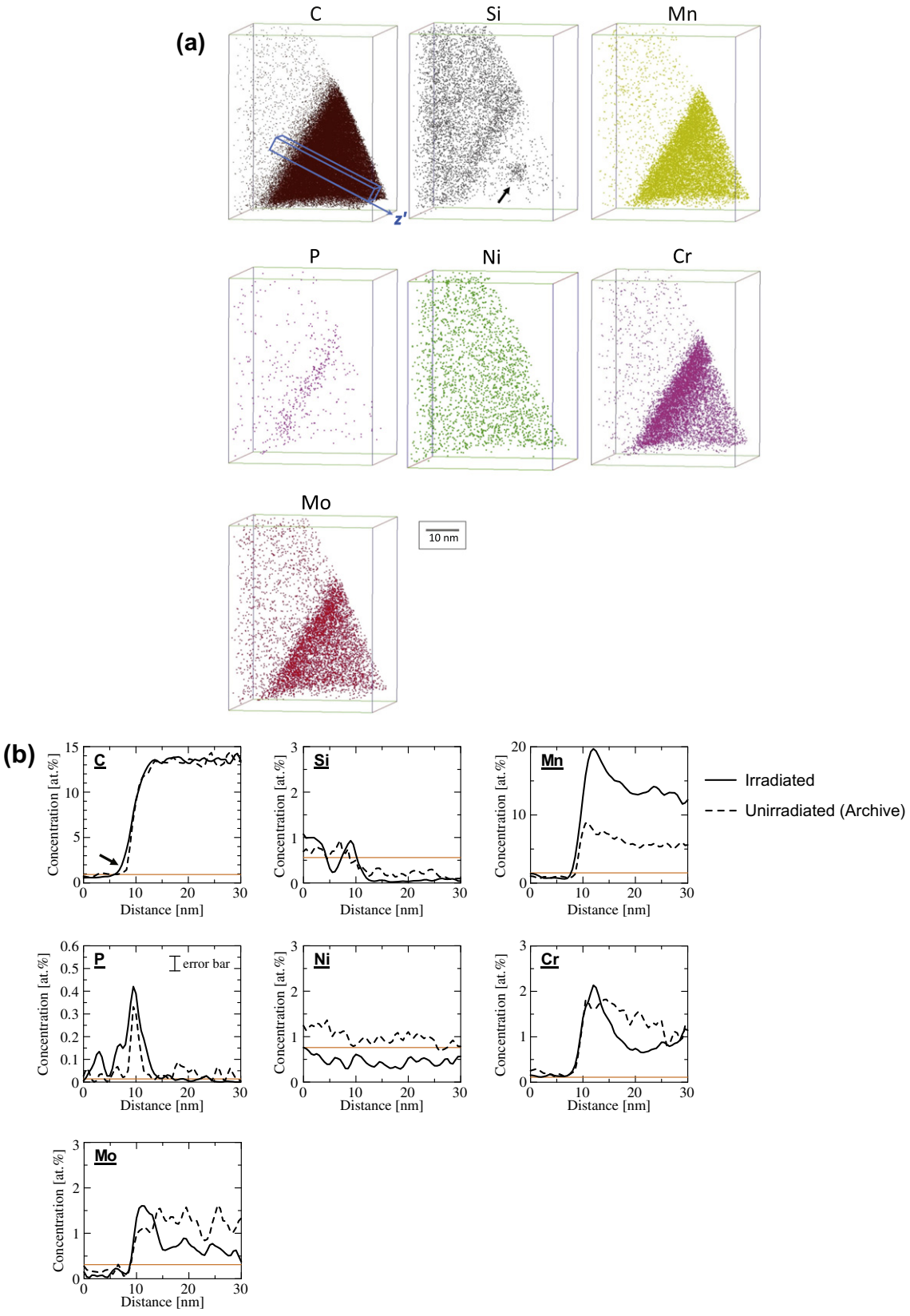

Fig. 2. (a) Elemental maps of solute atoms around the carbide in the neutron irradiated surveillance specimen, and (b) concentration profiles of each element as a function of position across the carbide–matrix interface in the selected region of a rectangular parallelepiped of 5 × 5 nm cross section in Fig. 2a. The concentration profiles around the carbide–matrix interface in the archive specimen (dashed lines) and the nominal concentrations of each element (orange lines) are also plotted for comparison.

almost the same as those of the archive specimen as mentioned above. Average atomic concentrations of the each element in the carbide other than the silicide were as follows; C: ~13%, Si: ~0.1%, Mn: ~14%, Ni: ~0.5%, Cr: ~1%, Mo: ~1% and balanced Fe (70%). The Mn concentration inside the carbide was increased after irradiation, whereas the Si, Ni and Mo concentrations inside the carbide was decreased. Subtotal concentration of the metal elements (Mn + Cr + Mo + Fe) was about 86%, which is close to that of M_6C type carbide and almost the same as that for the archive specimen.

Fig. 2b shows atomic concentrations of each element in the selected region in the C map in Fig. 2a, in the similar way as Fig. 1b. The concentration profiles of the archive specimen shown in Fig. 1b are also plotted by dashed lines for comparison. The Mn, Cr and Mo concentrations were further enhanced around the inner carbide–matrix interface by irradiation. In the similar way with the archive specimen, FWHM of the enhancement peaks of Mn, Cr and Mo at the interface ($z' \sim 10$ nm) were estimated to be ~4 nm, ~5 nm and ~4 nm, respectively. These FWHM are narrower than those of the archive specimen, showing that these enhancements are significantly intensified and sharpened by irradiation. Segregation of P at the carbide–matrix interface is also intensified by irradiation in the observed interface.

The nominal concentrations of each element, listed in Tab. 1, are also presented by horizontal orange lines in Fig. 2b. It should be empathized that the Mn and Mo concentrations in the matrix outside the carbide are lower than those nominal concentrations. It has been suggested that, in the low impurity RPV steels of the present study, Mn plays an important role for the irradiation-induced hardening by forming co-cluster with Si and Ni [26,27]. The observed depletion of Mn in the matrix might produce a cluster-free zone in the matrix adjacent to the carbide. It should be also noted that the Ni concentration both in matrix and the carbide decreased after irradiation. One of the reasons of this is the formation of Si–Mn–Ni clusters in matrix in the irradiated specimen; we have made other 3D-AP observation of the irradiated specimen and found Si–Mn–Ni clusters of a number density about 5×10^{16} cm^{-3} in matrix. The Si, Mn and Ni concentrations in matrix were decreased by irradiation; Si: 0.6 (archive) → 0.5 (irradiated), Mn: 1.4 → 1.2, Ni: 0.7 → 0.6 (in at.%). These results will be submitted elsewhere.

It is widely accepted that P segregation is responsible for brittleness of interfaces such as grain boundaries and carbide–matrix interfaces in RPV steels. Directly, a recent fracture toughness prediction model has reported that the strength of carbide–matrix interface is reduced by P segregation at the interface [6,11,12]. Thus the observed intensifying of P segregation by irradiation would decrease the interfacial strength. Furthermore, the strength of the interface is dependent on the atomic distributions around the interface in addition to P segregation: chemical composition and size of the impurity-concentrated zones near carbides [28]. In view of this, the observed intensifying of Mn, Cr and Mo enhancement and sharpening of these distributions by irradiation would also decrease the interfacial strength and hence degrade fracture toughness of RPV steels. Such contributions of the observed nanostructural changes in mechanical properties will be the subject of further discussion in a later paper.

The tailing of the step-like concentration profile of Mn, Cr, Mo from the carbide interface to the matrix in Fig. 2b ($z' \sim 10$ nm) is almost the same between the archive and the irradiated specimens. In contrast, the profile of C seems to be slightly smeared after irradiation as shown by the arrow. This smearing is possibly due to the dissolving of C from the carbide to matrix resulting from the migration of interstitial carbon atoms induced by irradiation.

4. Conclusion

Irradiation-induced changes of the atomic distributions around nano-scale carbides in the RPV steel of Doel-4 reactor in Belgium were investigated by laser-assisted local electrode-type 3D-AP. In the unirradiated specimen, nano-scale Fe–Mn–Cr–Mo carbides (~M_6C type) were observed. Mn, Cr and Mo were enriched around the inner carbide–matrix interface. The depletion of Si in the carbide and the segregation of P at the interface were also observed. By neutron irradiation for 12 years, the Mn concentration within the carbide was increased and the enhancement of Mn, Cr and Mo concentration around the carbide–matrix interface as well as P segregation at the interface were markedly intensified. These changes could be one of the possibilities for degradation of the interface, which would contribute to the embrittlement of RPV steels.

Acknowledgements

The authors would like to thank M. Narui and M. Yamazaki for their support for hot laboratory work and The Utility Electrabel for their permission to publish the present results on the surveillance test specimens. This work was partially supported by Grant-in-Aids for Scientific Research (Nos. 17002009, 20860018 and 20860018) and a research program of Nuclear Research, of the Ministry of Education, Culture, Sports, Science and Technology.

References

[1] W.J. Phythian, C.A. English, J. Nucl. Mater. 205 (1993) 162–177.
[2] G.R. Odette, Mater. Soc. Symp. Proc. 373 (1995) 137–148.
[3] R.G. Carter, N. Soneda, K. Dohi, J.M. Hyde, C.A. English, W.L. Server, J. Nucl. Mater. 298 (2001) 211–224.
[4] J.T. Buswell, W.J. Phythian, R.J. McElroy, S. Dumbill, P.H.N. Ray, J. Mace, R.N. Sinclair, J. Nucl. Mater. 225 (1995) 196–214.
[5] C.A. English, S.R. Ortner, G. Gage, W.L. Server, S.T. Rosinski, in: S.T. Ronsinski, M.L. Grossbeck, T.R. Allen, A.S. Kumar (Eds.), Effects of Radiation on Materials, ASTM STP 1405, ASTM, 2001, pp. 151–173.
[6] B.Z. Margolin, V.A. Shvetsova, A.G. Gulenko, V.I. Kostylev, Eng. Fract. Mech. 75 (2008) 3483–3498.
[7] J.A. Hudson, S.G. Druce, G. Gage, M. Wall, Theor. Appl. Fract. Mech. 10 (1988) 123–133.
[8] B.A. Gurovich, E.A. Kuleshova, Y.I. Shtrombakh, O.O. Zabusov, E.A. Krasikov, J. Nucl. Mater. 279 (2000) 259–272.
[9] B. Tanguy, J. Besson, R. Piques, A. Pineau, Eng. Fract. Mech. 72 (2005) 49–72.
[10] S.R. Bordet, B. Tanguy, J. Besson, S. Bugat, D. Moinereau, A. Pineau, Fatigue Fract. Eng. Mater. Struct. 29 (2006) 799–816.
[11] B.Z. Margolin, V.A. Shvetsova, A.G. Gulenko, V.I. Kostylev, Int. J. Press. Vess. Pip. 84 (2007) 320–336.
[12] B.Z. Margolin, V.A. Shvetsova, A.G. Gulenko, V.I. Kostylev, Fatigue Fract. Eng. Mater. Struct. 29 (2006) 697–713.
[13] W.J. Yang, B.S. Lee, Y.J. Oh, M.Y. Huh, J.H. Hong, Mater. Sci. Eng. A 379 (2004) 17–20.
[14] D.G. Park, E.J. Moon, D.J. Kim, S.H. Chi, J.H. Hong, Physica B 327 (2003) 315–320.
[15] M.K. Miller, M.G. Burke, J. Nucl. Mater. 195 (1992) 68–82.
[16] P. Pareige, J.C. Van Duysen, P. Auger, Appl. Surf. Sci. 67 (1993) 342–347.
[17] P. Pareige, K.F. Russell, R.E. Stoller, M.K. Miller, J. Nucl. Mater. 250 (1997) 176–183.
[18] M.K. Miller, P. Pareige, M.G. Burke, Mater. Charact. 44 (2000) 235–254.
[19] T.F. Kelly, M.K. Miller, Rev. Sci. Instrum. 78 (2007) 031101.
[20] K. Thompson, P.L. Flaitz, P. Ronsheim, D.J. Larson, T.F. Kelly, Science 317 (2007) 1370–1374.
[21] M.K. Miller, K.F. Russell, J. Nucl. Mater. 371 (2007) 145–160.
[22] X. Jiang, X. Xie, Z. Xu, Surf. Coat. Technol. 168 (2003) 156–160.
[23] C. Zhu, X.Y. Xiong, A. Cerezo, R. Hardwicke, G. Krauss, G.D.W. Smith, Ultramicroscopy 107 (2007) 808–812.
[24] F.G. Caballero, M.K. Miller, S.S. Babu, C. Garcia-Mateo, Acta Mater. 55 (2007) 381–390.
[25] F.G. Caballero, M.K. Miller, C. Garcia-Mateo, C. Capdevila, S.S. Babu, Acta Mater. 56 (2008) 188–199.
[26] G.R. Odette, B.D. Wirth, J. Nucl. Mater. 251 (1997) 157–171.
[27] G.R. Odette, G.E. Lucas, JOM 53 (2001) 18–22.
[28] B.Z. Margolin, A.G. Gulenko, V.A. Nikolaev, L.N. Ryadkov, Int. J. Press. Vess. Pip. 82 (2005) 679–686.